Center and Characteristic Seismic Reliability as new indexes for accounting uncertainties in seismic reliability analysis

(Article begins on next page)

Center and characteristic seismic reliability as new indexes for accounting uncertainties in seismic reliability analysis

Mariano Angelo Zanini [a, *], Lorenzo Hofer [a]

[a] *Department of Civil, Environmental and Architectural Engineering, University of Padova, via Francesco Marzolo 9, Padova, Italy*

ARTICLE INFO

ABSTRACT

Seismic reliability analysis is a powerful tool to assess structural safety against ground shaking actions induced by earthquake occurrences. The classic approach for computing seismic reliability of a structural system requires a seismic hazard curve and a fragility function and leads to the estimation of the failure probability of the investigated damage state. However, resulting failure probability is strongly related to the preliminary assumptions in both hazard and fragility analyses, and slight changes in the input model parameters may cause relevant variability of seismic reliability estimates. The present work formalizes a general approach to be followed when dealing with seismic reliability assessment of structural systems, aimed at taking into account the whole uncertainties of the input parameters within hazard and fragility models. In the proposed approach, probability of failure becomes in turn a random variable and therefore new indexes are introduced, namely *Expected Failure Rate*, *Failure Rate Dispersion*, *Characteristic Failure Rate*, *Center of Seismic Reliability* and *Characteristic Seismic Reliability*. Lastly, such approach is applied to a case study, where seismic reliability of an existing open-spandrel reinforced concrete arch bridge is analyzed, and results are discussed highlighting some relevant issues.

1. Introduction

Research and practical applications in earthquake engineering are increasingly oriented at adopting concepts underlying the design of structures with reference to a set of performance targets. This implies that engineers have to ensure the structural system to meet adequate safety levels during the entire service-life. Structural safety is usually quantified via the execution of a reliability analysis [1], using alternatively analytical (e.g. First or Second Order Reliability Methods [2,3]) or numerical (e.g. Monte Carlo simulations [4], Importance Sampling [5,6], Directional Sampling [7], Subset simulation [8], Latin Hyper-Cube Method [9–11]) approaches depending on the complexity of the structural system of interest. The main aim of a reliability analysis is therefore to assess structural safety [12], accounting for all the sources of variability - both in load and resistance models - and their impact on structural performance, and thus computing the failure probability [13]. Failure probability represents in fact the metric of structural safety, i.e. the probability to meet or exceed a target performance level or damage state [14]. However, failure probability estimates are

strongly related to assumed models and input data at both hazard and fragility sides, since both the models themselves and their parameters are uncertain. This issue is mainly due to an incomplete knowledge of such processes (i.e., the so-called epistemic uncertainty). Quantifying the impact of uncertainties in seismic reliability and risk analysis is therefore an emerging challenge that researchers in earthquake engineering are asked to address, since a specific scientific literature is still scarce.

Some uncertainty assessments were carried out in previous research works within the context of seismic hazard analysis, pointing out a clear distinction between aleatory and epistemic uncertainties [15–17]. In the current practice of Probabilistic Seismic Hazard Analysis (PSHA), one of the most widely adopted method for addressing hazard epistemic uncertainty is the so-called logic tree approach [18], in which every node represents a potential source of epistemic uncertainty, and the corresponding outcoming branches represent the possible alternatives. Through the logic tree approach, it is possible to consider both the intra- and the inter-model uncertainties, the former due to uncertainty in the model parameters, the latter for describing the uncertainty among models. Despite its wide adoption in PSHA [19], the use of logic trees is often debated, due to potential drawbacks [20]. In particular,

* Corresponding author.
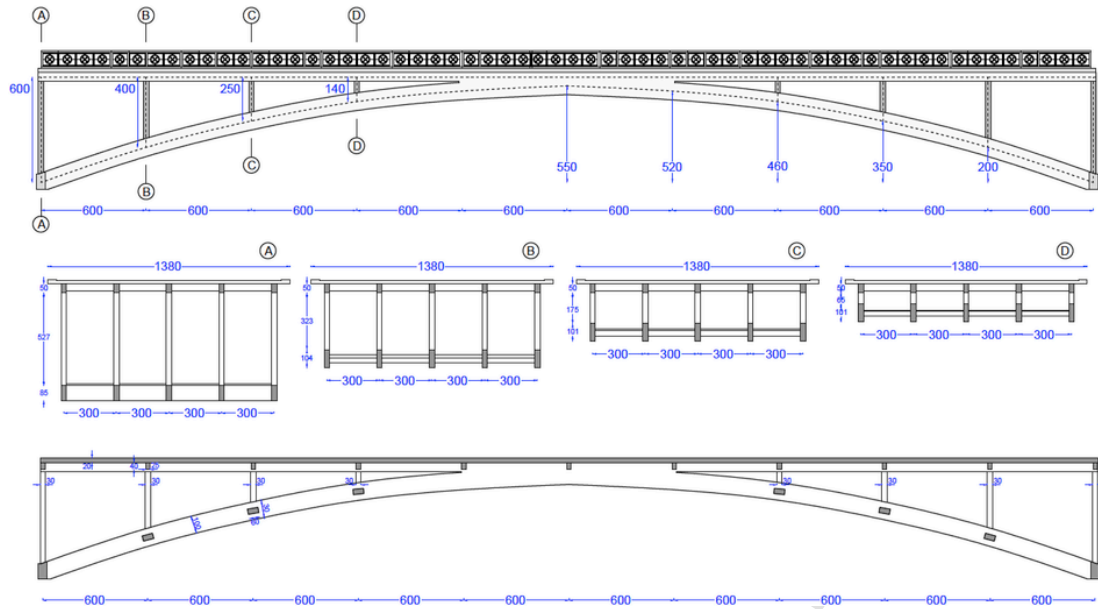 *Email address:* marianoangelo.zanini@dicea.unipd.it (M.A. Zanini).

Fig. 1. RC arch bridge: elevation, transversal and longitudinal sections.

Table 1
Uncertainty characterization of hazard $\mathbf{\Theta}_H$ model parameters.

$\mathbf{\Theta}_H$				
Parameter		Mean	COV	Distribution type
SZ # 903	$\Upsilon_{m_{min}}$	0.117	0.1	Normal
	B	1.786	0.1	Normal
	M_{min}	4.3	0.01	Normal
	M_{max}	5.8	0.1	Normal
SZ # 904	$\Upsilon_{m_{min}}$	0.050	0.1	Normal
	B	0.939	0.1	Normal
	M_{min}	4.3	0.01	Normal
	M_{max}	5.5	0.1	Normal
SZ # 905	$\Upsilon_{m_{min}}$	0.316	0.1	Normal
	B	0.853	0.1	Normal
	M_{min}	4.3	0.01	Normal
	M_{max}	6.6	0.1	Normal
SZ # 906	$\Upsilon_{m_{min}}$	0.135	0.1	Normal
	B	1.092	0.1	Normal
	M_{min}	4.3	0.01	Normal
	M_{max}	6.6	0.1	Normal
SZ # 907	$\Upsilon_{m_{min}}$	0.065	0.1	Normal
	B	1.396	0.1	Normal
	M_{min}	4.3	0.01	Normal
	M_{max}	5.8	0.1	Normal
SZ # 912	$\Upsilon_{m_{min}}$	0.091	0.1	Normal
	B	1.004	0.1	Normal
	M_{min}	4.3	0.01	Normal
	M_{max}	6.1	0.1	Normal
$\mathbf{\Theta}_{GMPE}$	Σ_{logPGA}	0.337	0.1	Normal

logic-tree results can be interpreted in two different ways. In the first case, logic tree branches are assumed to fully represent all possible hazard outcomes, and the alternative branches represent a mutually exclusive and collectively exhaustive set of events. With this interpretation, the only result is the mean hazard [21–23]. In the second case, percentiles associated to the logic tree outcomes are used for describing hazard uncertainty through the discrete distribution of final branches' outputs [24,25]. In 2015, Marzocchi et al. [26] proposed a general framework called ensemble modelling, in which the logic tree is treated as a technical tool for sampling epistemic uncertainty. Finally, an extensive discussion on the proper scientific interpretation of seismic hazard estimates can be found in Marzocchi and Jordan [27]. In any case, logic tree results strictly depend on how logic tree branches

are populated, and on the weight assigned to each branch [28]. In this regard, Sabetta et al. [29] showed how the selection of appropriate ground motions prediction equations (GMPE) has a significant impact on results, more than the expert judgement applied in assigning relative weights to the logic tree branches. Bommer and Abrahamson [30] demonstrated how aleatory uncertainty in GMPE has a pronounced influence on the computed hazard.

Some studies were also carried out in order to analyze the impact of finite element (FE) model selection and modelling simplifications [31–33], record selection [34–36], and the impact of uncertainty in FE modelling parameters on the seismic fragility estimates [37–39]. Among others, Liel et al. [40] performed a detailed assessment of collapse risk of reinforced-concrete (RC) moment frame buildings, focusing on the impact of modelling parameters in terms of material strengths of structural components, as well as other properties like stiffness, deformation capacity and cyclic deterioration on the resulting seismic fragility estimates. Oh-Sung and Elnashai [41] provided some insights in demonstrating how record selection seems to be the mostly affecting source of uncertainty, if compared to the effects of randomness linked to material parameters. Dolsek [42] studied the impact of epistemic uncertainties on the computation of fragility curves of a four-story RC frame, with the Incremental Dynamic Analysis (IDA) approach, by randomly generating a set of sample structural models with the Latin HyperCube Method. In his study, Dolsek showed how the impact of epistemic uncertainties seems to affect seismic response parameters mainly with reference to collapse capacity, rather than to less relevant damage states. Celik and Ellingwood [43] examined the contribution of uncertainties in material and structural parameters for different non-ductile RC frames, showing how structural damping, concrete strength, and cracking strain in beam-column joints had the greatest impact on the fragilities. The authors also evidenced how the resulting curves were quite similar from those based solely on the uncertainty in seismic demand from earthquake ground motion. This outcome suggested that fragilities developed assuming that all structural parameters are deterministic, and equal to their median values, are sufficient for purposes of earthquake damage and loss estimation, in regions of moderate seismicity. More recently, Scozzese et al. [44] assessed the impact of uncertainties related to the material and mechanical characterization of isolators and dampers, investigating their propagation up to the risk estimation by means of a novel optimization ap-
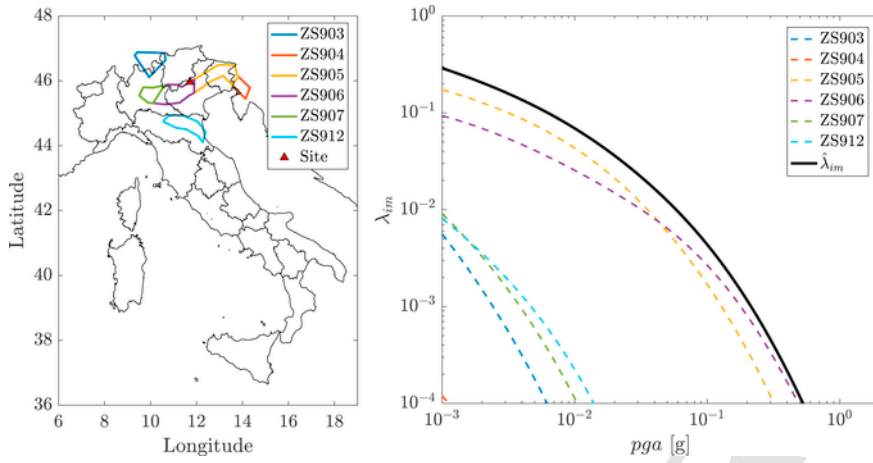
Fig. 2. Bridge site, adopted seismogenic source model and PSHA results.
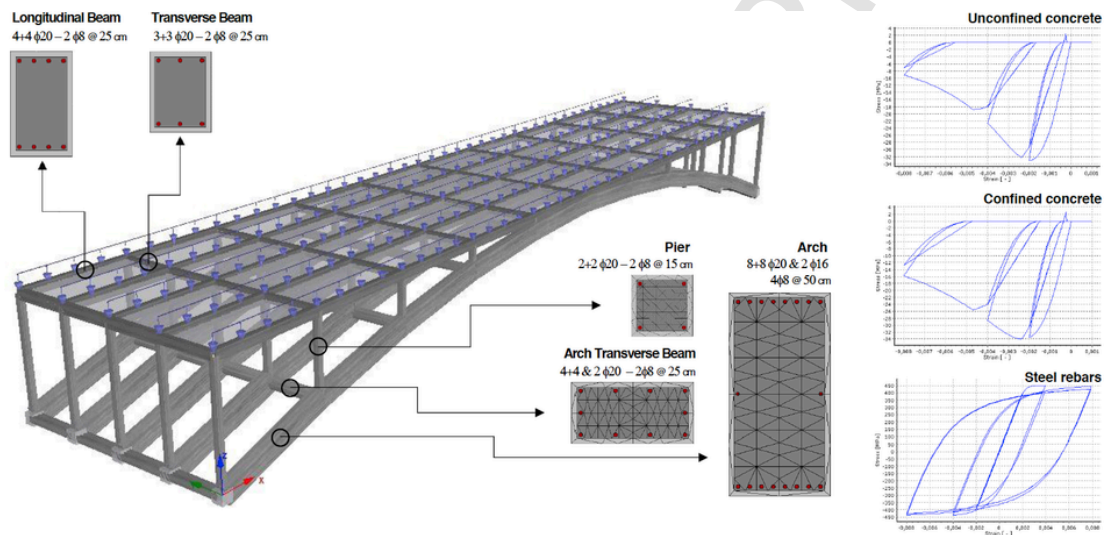

Fig. 3. RC arch bridge FE model and adopted constitutive laws for unconfined - confined concrete and steel rebars.

proach. Jiang and Ye [45] showed how the 50-years collapse probability of failure of a two-story steel building considering uncertainties linked to record selection, structural modelling and in the definition of performance limits, is 1.84–4.56 times higher than the value derived solely considering record-to-record variability.

However, despite the growing attention on such topic, there is a substantial lack of a general approach to be conventionally followed in order to quantify the impact of uncertainties in seismic reliability analysis. As previously reported, epistemic uncertainties associated to both hazard and fragility were always separately considered in literature studies, without any indication on the prevailing source of randomness when assessing seismic reliability that considers both.

For the abovementioned reasons, the present work illustrates, as main novelty element, a general approach for the seismic reliability assessment, able to investigate the uncertainty of λ_f arising from epistemic uncertainties linked to both hazard and fragility models, based on the formalization of the dependence of $\lambda_f(\Theta)$ on model parameters Θ. The proposed general approach allows quantifying the degree of belief that the risk analyst has for a certain seismic reliability estimate, on the basis of the uncertainties' levels existing in the assumption of both hazard and fragility model parameters. As a further novelty element, the paper proposes some new seismic reliability indexes, namely Expected Failure Rate, Failure Rate Dispersion, Characteristic Failure Rate, Center of Seismic Reliability and Characteristic Seismic Reliabil-

ity, for communicating the failure rate uncertainty and using results of the uncertainty analysis for design/assessment purposes. The paper is structured as follows: Section 2 reviews the sources of uncertainty linked to both hazard and fragility assessment methods currently in use, while Section 3 is devoted to the formalization of the dependence of $\lambda_f(\Theta)$ on model parameters Θ and the definition of the newly proposed seismic reliability indexes. In the second part of the work, Section 4 describes in detail a case study represented by an existing open-spandrel RC arch bridge for which the proposed general approach to seismic reliability assessment is applied, whose results are illustrated in Section 5. Lastly, Section 6 presents an in-depth discussion of the results obtained from the case study aimed at highlighting the prevailing source of randomness, and the impact of such uncertainties when looking at different damage states.

2. Uncertainties in the failure rate computation

In this Section, an overview on the sources of uncertainty linked to both hazard and fragility assessment methods currently in use is provided. In the Performance-Based Earthquake Engineering (PBEE) framework [46], the occurrence of the main earthquakes at the construction site is commonly assumed to be a Homogenous Poisson Process (HPP). Under this hypothesis, and not considering damage accumulation on structures, the process of events causing the structural
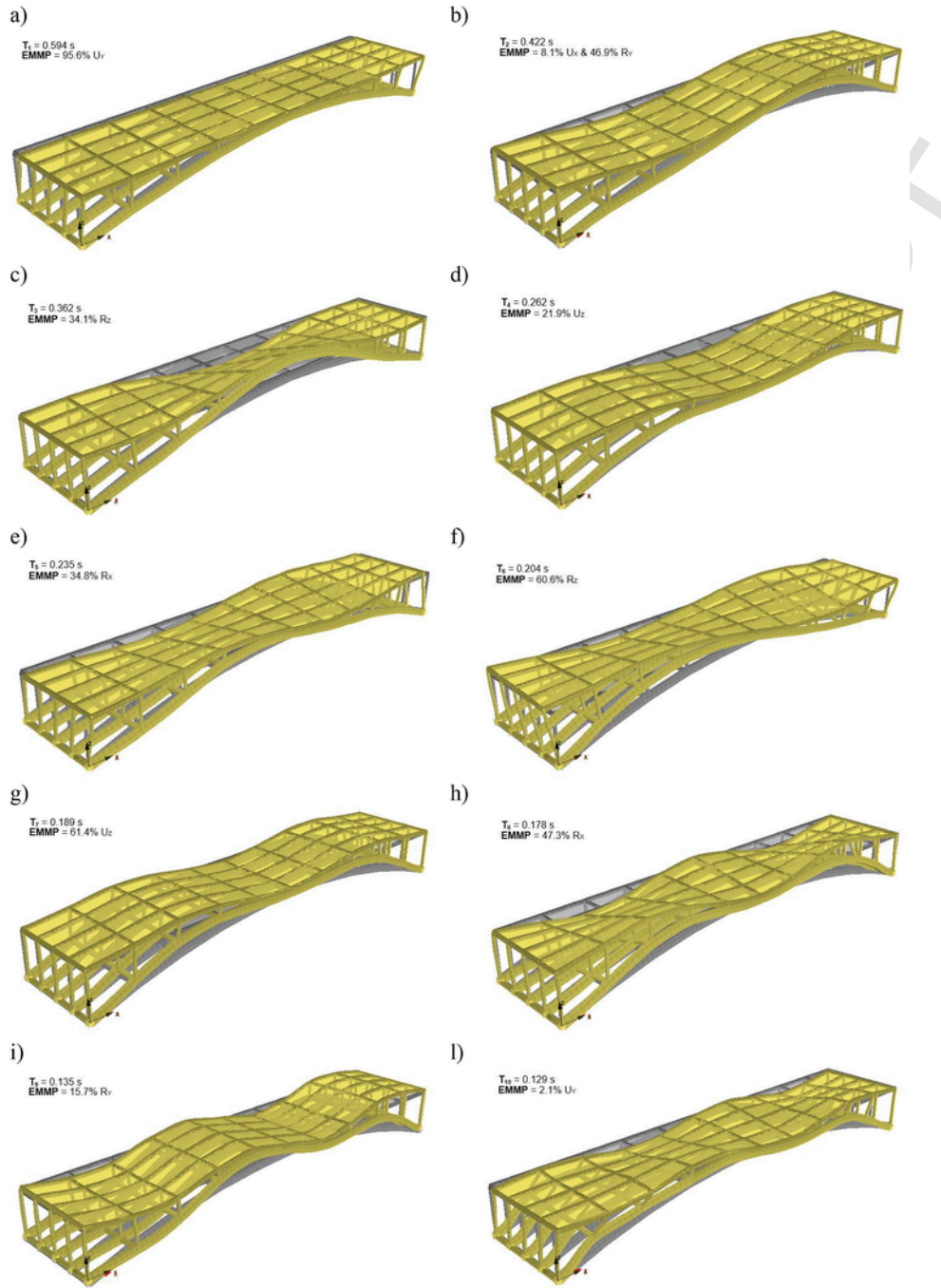
Fig. 4. RC arch bridge main vibration modes and EMMP values.

failure is also represented by an HPP, whose unique parameter, the failure rate λ_f, can be used for computing the failure probability in any time interval. For this reason, the failure rate λ_f represents one of the most used risk indicators, mainly due to its simplicity and its unique dependence on the seismic hazard and on the structural behavior. It is computed as:

$$\lambda_f = \int_{im} P\left[f|im\right] \cdot \left|d\lambda_{im}\right| \tag{1}$$

where λ_{im} is the *hazard curve* and represents the seismicity at a specific site, whereas the $P[f|im]$ is the *fragility curve* and it characterizes the probabilistic structural behavior of a structural system (probability of reach and exceed a specific damage level). Current state-of-the-art ap-

proaches for the computation of λ_{im} are based on PSHA [47,48], which associates to each ground motion intensity measure $IM = im$ value, the corresponding annual rate of events exceeding im at the site where the structure is located. The most widely adopted intensity measure IM is the peak ground acceleration (PGA), i.e. the spectral acceleration corresponding to a structural period equal to zero; however, for specific applications, spectral accelerations for other different structural period can be used. In Eq. (1) λ_{im}, $\left|d\lambda_{im}\right|$ can be easily obtained as the derivative of the hazard curve:

$$\left|d\lambda_{im}\right| = -\frac{d\lambda_{im}}{d\left(im\right)}d\left(im\right) \tag{2}$$

$P[f|im]$ represents the probability of reach and exceed a specific dam-

Table 2
Selected 3-D earthquake records.

| Record ID	Event	Date	M_w	R [km]	PGA_H [g]	PGA_Z [g]
1	L'Aquila	06/04/2009	6.1	4.9	0.770	0.496
2	L'Aquila	06/04/2009	6.1	5.0	0.448	0.443
3	Emilia-Romagna	29/05/2012	6.0	0.5	0.441	0.349
4	L'Aquila	06/04/2009	6.1	5.1	0.491	0.240
5	Friuli	17/06/1976	5.2	14.3	0.090	0.008
6	Friuli	11/09/1976	5.6	18.6	0.239	0.090
7	Southern Italy	16/01/1981	5.2	21.7	0.109	0.022
8	Umbria-Marche	14/10/1997	5.6	40.7	0.044	0.015
9	Northern Italy	07/06/1980	4.6	11.3	0.060	0.037
10	Duzce	12/11/1999	7.3	36.1	0.908	0.195
11	Duzce	12/11/1999	7.3	27.4	1.030	0.323
12	Central Italy	26/10/2016	5.4	3.7	0.757	0.304
13	Turkey	01/05/2003	6.3	11.8	0.527	0.432
14	Western Caucasus	03/05/1991	5.6	17.8	0.563	0.103
15	Pyrgos	26/03/1993	5.4	1.3	0.469	0.076
16	Southern Greece	15/09/1986	4.8	14.3	0.335	0.124
17	Greece	08/11/2014	5.1	9.2	0.403	0.089
18	Greece	24/04/1988	4.2	16.4	0.280	0.039
19	Greece	19/05/1995	5.1	15.1	0.284	0.122
20	Greece	14/07/1993	5.6	4.9	0.410	0.127
21	Azores Islands	09/07/1998	6.2	13.3	0.433	0.304
22	Greece	07/09/1999	5.9	26.3	0.158	0.080
23	Albania	13/06/1993	5.3	58.5	0.148	0.035
24	Central Italy	26/01/2003	4.7	7.9	0.130	0.066
25	Southern Greece	25/10/1984	5.0	15.6	0.193	0.087
26	Friuli	11/09/1976	5.2	6.1	0.201	0.077
27	Norcia	19/09/1979	5.8	40.4	0.085	0.016
28	Friuli	06/05/1976	6.4	27.7	0.392	0.273
29	Ancona	14/06/1972	4.2	9.3	0.433	0.157
30	Gibraltar	04/01/1994	4.9	24.4	0.062	0.045

age level, conditioned on a specific *im* value. The *fragility curve* $P[f|im]$ is strongly influenced by the type of analyzed structural system, and its calibration is commonly based on results carried out with a set of non-linear dynamic analyses. Among all procedures proposed in literature for the calibration of $P[f|im]$ parameters, the most used are the Incremental Dynamic Analysis (IDA, [49]), the Cloud-Analysis (CA, [50]), and the Multi-Stripes Analysis (MSA, [51]). λ_f computed with Eq. (1) is a point estimate of the failure rate, that derives from specific assumed parameters both in λ_{im} and in $P[f|im]$. In this context, λ_f is thus function of a set of parameters Θ contained in both the *hazard* (Θ_H) and in the *fragility curve* (Θ_F). When these model parameters $\Theta = [\Theta_H; \Theta_F]$ are assumed to be random variables (RVs), the failure rate itself becomes a RV with unknown distribution and moments.

2.1. Hazard curve uncertainties

The hazard curve λ_{im} is commonly computed via the PSHA integral as:

$$\lambda_{im} = \sum_{i=1}^{n_{SZ}} \upsilon_{m_{min,i}} \int_{m_{min,i}}^{m_{max,i}} \int_{r_{min,i}}^{r_{max,i}} P[IM > im|m,r] f_{M_i}(m) f_{R_i}(r) \, dm \, dr \quad (3)$$

where $\upsilon_{m_{min,i}}$ is the rate of occurrence of earthquakes greater than a suitable minimum magnitude $m_{min,i}$ of the *i*th seismogenic zone (*SZ*), $f_{M_i}(m)$ is the magnitude distribution for the *i*th *SZ* and $f_{R_i}(r)$ is the distribution of the source *i*th-to-site distance. Finally, $P[IM > im|m,r]$ represents the probability to exceed the value *im* at the site of interest due to a seismic event with magnitude *m* occurring at a certain epicenter-to-site distance *r*. $P[IM > im|m,r]$ is usually computed with a Ground Motion Prediction Equation (GMPE), which predicts the probability distribution of an *IM* of interest as a function of many input variables, like magnitude, source-to-site distance, soil type, faulting style. Model parameters to be treated as RVs can be found involved in the hazard computation, in all the above terms. When a truncated Gutenberg–Richter (G-R) occurrence law [52,53] is adopted for the *i*th *SZ*, the magnitude distribution $f_{M_i}(m; \Theta_M)$ depends on the parameters vector $\Theta_M = [M_{max,i}, M_{min,i}, B_i]$, where $M_{max,i}$ and $M_{min,i}$ represent the magni-
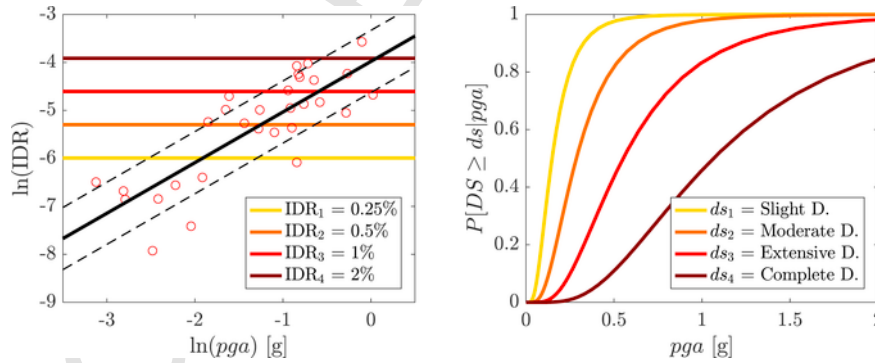
Fig. 5. Cloud analysis results and related analytical fragility curves.
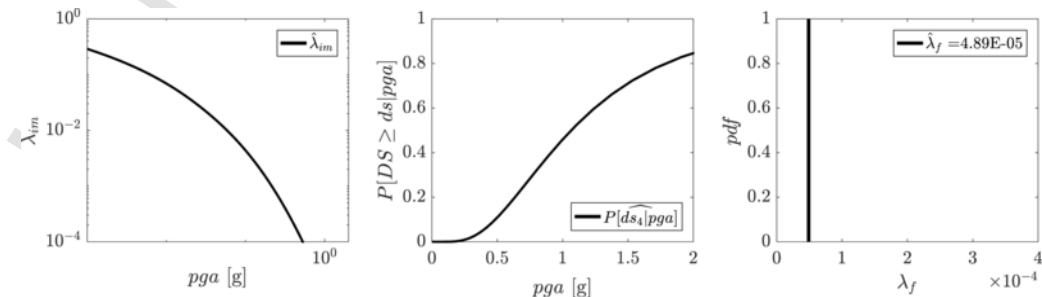
Fig. 6. Classic seismic failure rate estimation for Complete DS.

Table 3

Uncertainty characterization of fragility $\mathbf{\Theta}_F$ model parameters.

$\mathbf{\Theta}_F$			
Parameter	Mean	COV	Distribution type
A_1	−3.979	0.055	Bivariate Normal
A_2	1.055	0.134	
Correlation coefficient	*a, b*	0.842	
B^2	0.42	0.267	Normal

tude interval of events that can occur in *SZ*, and B_i represent the slope of the G-R relationship. Also $Y_{M_{min,i}}$ of Eq. (3) can be considered as random and it is included among model parameters $\mathbf{\Theta}_M$ related to the G-R law. Similarly to $f_{M_i}(m;\mathbf{\Theta}_M)$, also $f_{R_i}(r;\mathbf{\Theta}_R)$ could be characterized by random parameters $\mathbf{\Theta}_R$, e.g. the fault length, in case that a linear source model is assumed, the fault diameter, for a circular *SZ*, or the

fault depth. Finally, the term $P[IM > im|m,r;\mathbf{\Theta}_{GMPE}]$ depends on the GMPE regression coefficients involved to compute the distribution parameters of the *im* expected in the specific site. Usually $\mathbf{\Theta}_{GMPE}$ includes a factor representing the soil type, the style of faulting, or other regression coefficients. Considering all the possible uncertainty sources involved in the hazard curve computation, Eq. (3) can be rewritten as:

$$\lambda_{im}\left(\mathbf{\Theta}_H\right) = \sum_{i=1}^{n_{SZ}} Y_{M_{min,i}} \int_{M_{min,i}}^{M_{max,i}} \int_{R_{min,i}}^{R_{max,i}} P\left[IM > im|m,r;\mathbf{\Theta}_{GMPE}\right] f_{M_i}\left(m;\mathbf{\Theta}_M\right) f_R$$

Note the general form of this notation, which allows including also the epistemic uncertainty related to the adoption of different GMPEs or different earthquake occurrence models, by simply introducing a *probability mass function* weighting each possible alternative. In this way, the classical *logic tree approach* [18,23] is included in the proposed formulation.
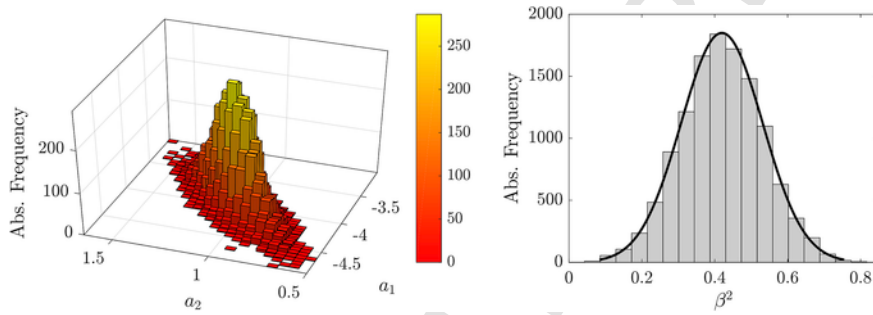

Fig. 7. $\mathbf{\Theta}_F$ fragility parameters sampling.
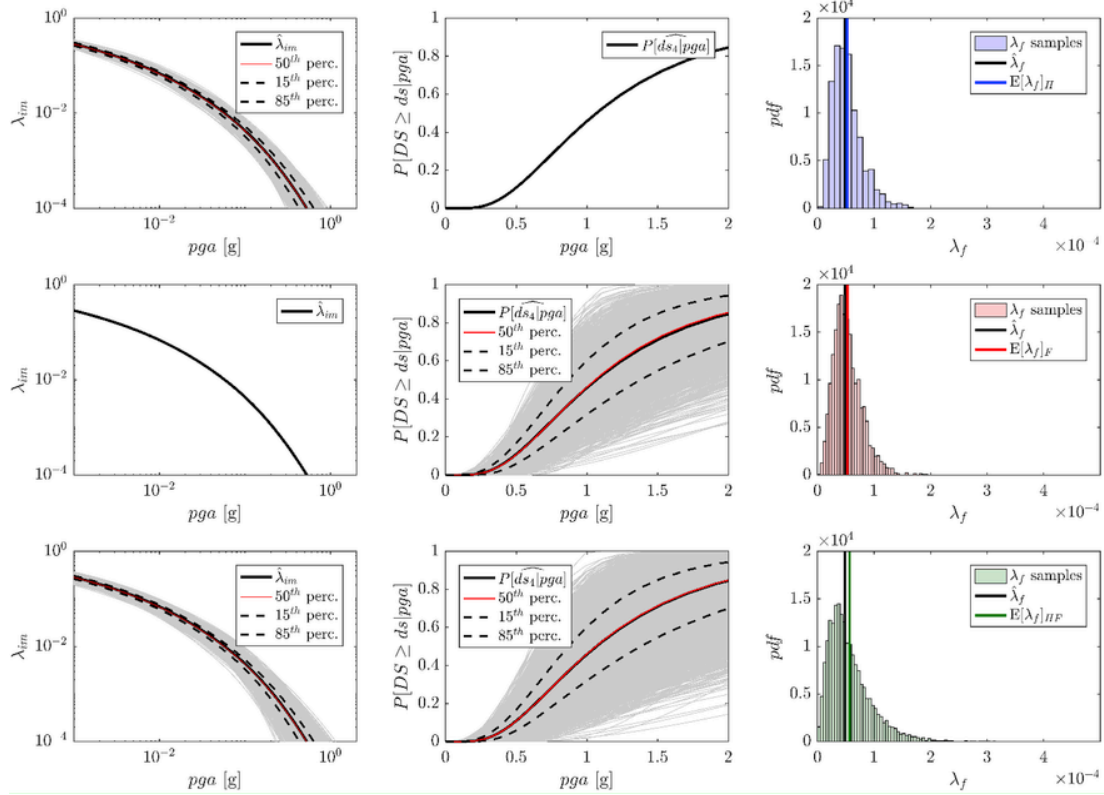

Fig. 8. Failure rate samples $\lambda_{f,i}$ obtained considering H (blue), F (red) and HF (green) uncertainties. (For interpretation of the references to colour in this figure legend, the reader is referred to the Web version of this article.)
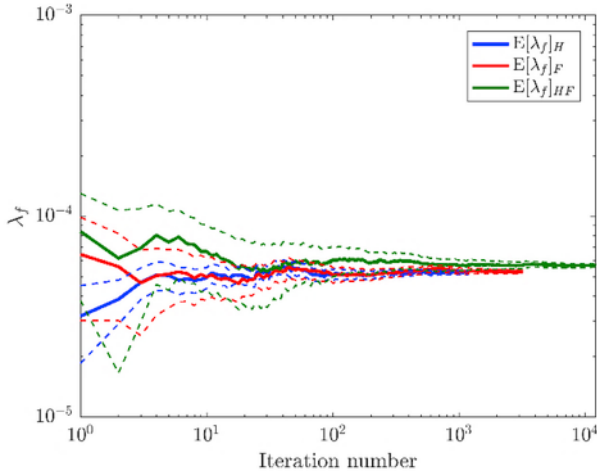
Fig. 9. Number of iterations for MCS convergence: H (blue), F (red) and HF (green) cases. (For interpretation of the references to colour in this figure legend, the reader is referred to the Web version of this article.)

2.2. Fragility curve uncertainty

The fragility function $P[f|im]$ is usually derived from results of non-linear dynamic analysis performed with specific structural software. Simulations are needed for obtaining a sample of structural responses for a given set of selected ground motions. Structural responses are usually quantified by setting an engineering demand parameter (EDP) of interest, i.e. a metric that can be used to estimate damage to structural (and/or non-structural) components. Common EDPs may be the inter-story drift, the pier-top displacement etc. Such data are further used to calibrate the relationship between the ground shaking level and the EDP of interest, i.e. the Probabilistic Seismic Demand Model (PSDM), able to capture non-linear seismic behavior of a structural system for increasing ground shaking levels [54,55]. Consequently, only an estimate of the fragility curve is obtained, since it is expected to change when varying the input ground motions sample. Several procedures can be found in literature for estimating the fragility parameters from structural analysis [51], among all the most adopted ones are the *IM-based* Incremental Dynamic Analysis (IDA) approach and the Cloud analysis approach.

In the first case, a set of n IDA curves, are used for drawing a sample of n intensity measures $[im_1, im_2, ..., im_n]$, at which the structural response reaches a specific undesired threshold level $\overline{edp}$ of engineering demand parameter (EDP). Each im_i can be seen as a realization of the random variable IM_f, i.e. of ground motion intensities that cause the reaching of the investigated structural damage level. Thus, the structural fragility can be computed as the probability of the RV IM_f to do not exceed the specific im value. In the case that the RV $ln(IM_f)$ is normally distributed, as commonly assumed in most of PBEE applications and widely proved in literature [56–58], $\mu_{ln(IM_f)}$ and $\sigma_{ln(IM_f)}$ represent respectively the mean and the standard deviation of $ln(IM_f)$ distribution. When these two parameters are treated as RVs, the following
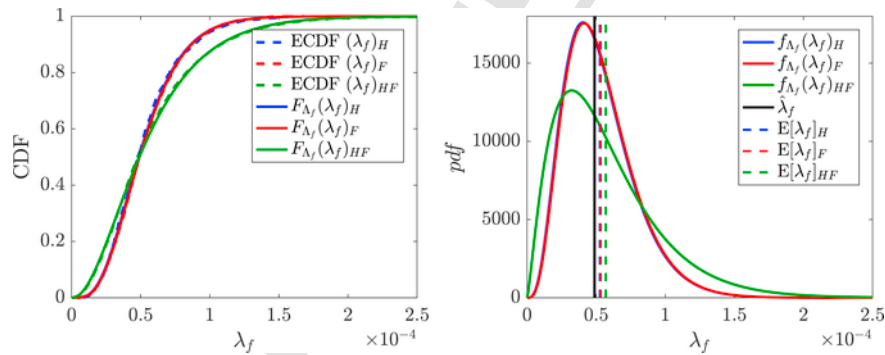
Fig. 10. Failure rate *pdf* $f_{\Lambda_f}(\lambda_f)$ fitting and comparison between $F_{\Lambda_f}(\lambda_f)$ and the empirical CDF.
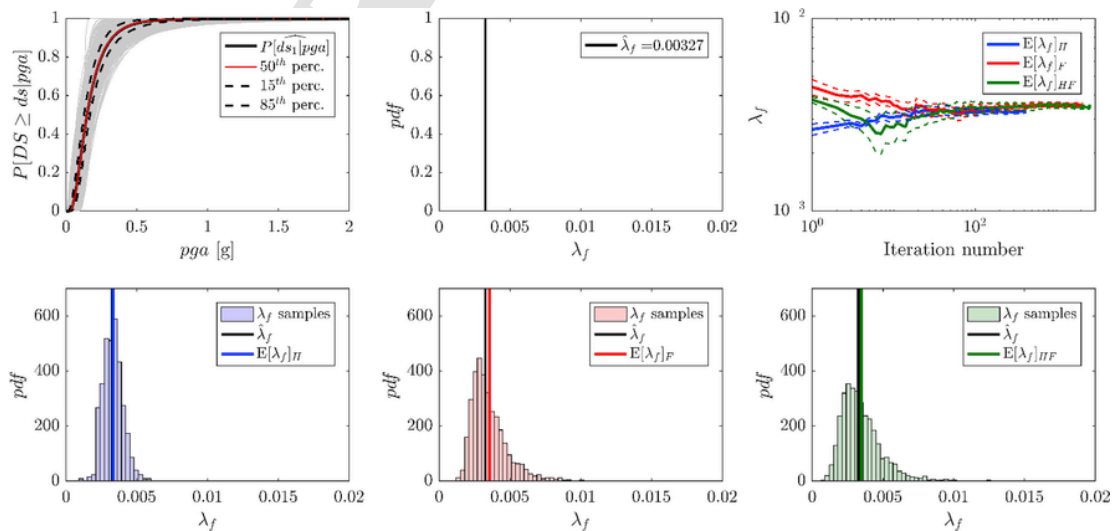

Fig. 11. Slight DS: sampled fragilities, $\hat{\lambda}_f$ point estimate, number of iterations for MCS convergence, and H (blue), F (red) and HF (green) failure rate samples $\lambda_{f,i}$. (For interpretation of the references to colour in this figure legend, the reader is referred to the Web version of this article.)
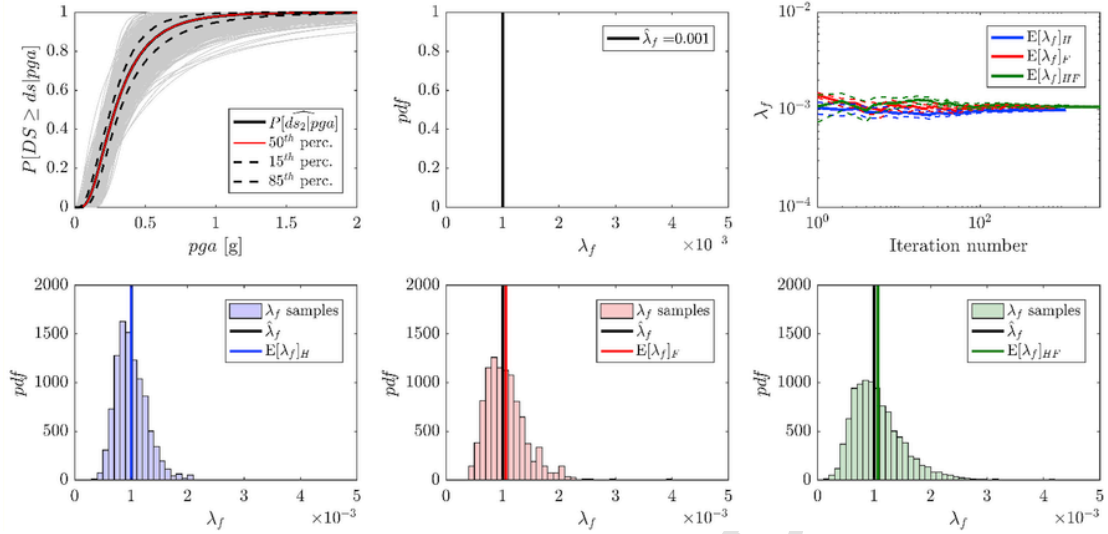
Fig. 12. Moderate DS: sampled fragilities, $\widehat{\lambda}_f$ point estimate, number of iterations for MCS convergence, and H (blue), F (red) and HF (green) failure rate samples $\lambda_{f,i}$. (For interpretation of the references to colour in this figure legend, the reader is referred to the Web version of this article.)
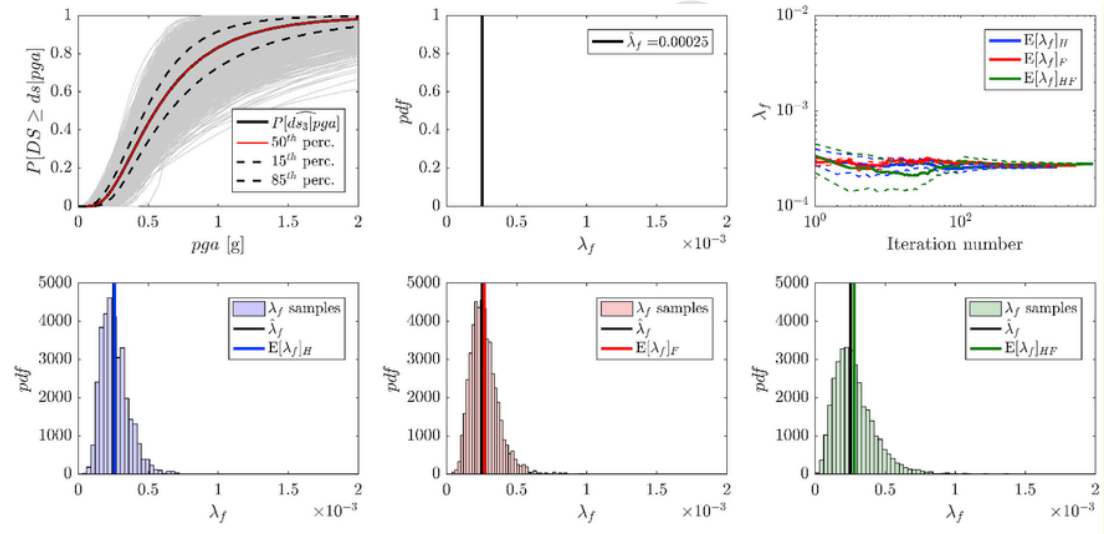
Fig. 13. Extensive DS: sampled fragilities, $\widehat{\lambda}_f$ point estimate, number of iterations for MCS convergence, and H (blue), F (red) and HF (green) failure rate samples $\lambda_{f,i}$. (For interpretation of the references to colour in this figure legend, the reader is referred to the Web version of this article.)

equation for the structural fragility can be derived

$$P\left[f|im;\mathbf{\Theta}_F\right] = P\,IM_f \leq im;\mathbf{\Theta}_F = \Phi\left[\frac{ln\,(im) - \mu_{ln\left(IM_f\right)}}{\sigma_{ln\left(IM_f\right)}}\right] \text{with } \mathbf{\Theta}_F = \left[M_{ln\left(IM_f\right)}, \Sigma\right.$$

From a sample $[im_1,\ im_2, ...,\ im_n]$ of n ground motion values, obtained with structural analysis, it is possible to derive a point estimate of $M_{ln(IM_f)}$ and $\Sigma_{ln(IM_f)}$ as:

$$\widehat{\mu}_{ln\left(IM_f\right)} = \frac{1}{n}\sum_{i=1}^{n} ln\left(im_i\right) \tag{6}$$

$$\widehat{\sigma}^2_{ln\left(IM_f\right)} = \frac{1}{n-1}\sum_{i=1}^{n}\left[ln\left(im_i\right) - \widehat{\mu}_{ln\left(IM_f\right)}\right]^2 \lim_{x\to\infty} \tag{7}$$

and thus, a point estimate $P\left[f|im;\widehat{\mathbf{\Theta}}_F\right]$ of the fragility function $P[f|im;\mathbf{\Theta}_F]$:

Furthermore, an approximated value for the variance of the mean $\widehat{\mu}_{ln\left(IM_f\right)}$ and variance $\widehat{\sigma}_{ln\left(IM_f\right)}^2$ estimator, can be computed as:

$$VAR\left[\widehat{\mu}_{ln\left(IM_f\right)}\right] \approx \frac{\widehat{\sigma}^2_{ln\left(IM_f\right)}}{n} \tag{8}$$

$$VAR\left[\widehat{\sigma}_{ln\left(IM_f\right)}^2\right] \approx \frac{2\cdot\widehat{\sigma}^4_{ln\left(IM_f\right)}}{n-1} \tag{9}$$

Regarding the Cloud Analysis approach, similar considerations on the model parameters can be done. In this case, the fragility computation takes origin from a sample of n ground motions intensities $[im_1,\ im_2, ...,\ im_n]$ and the corresponding sample of structural responses $[edp_1,\ edp_2, ...,\ edp_n]$. In this case, the fragility function assumes the fol-

Fig. 14. Complete DS: sampled fragilities, $\widehat{\lambda}_f$ point estimate, number of iterations for MCS convergence, and H (blue), F (red) and HF (green) failure rate samples $\lambda_{f,i}$. (For interpretation of the references to colour in this figure legend, the reader is referred to the Web version of this article.)
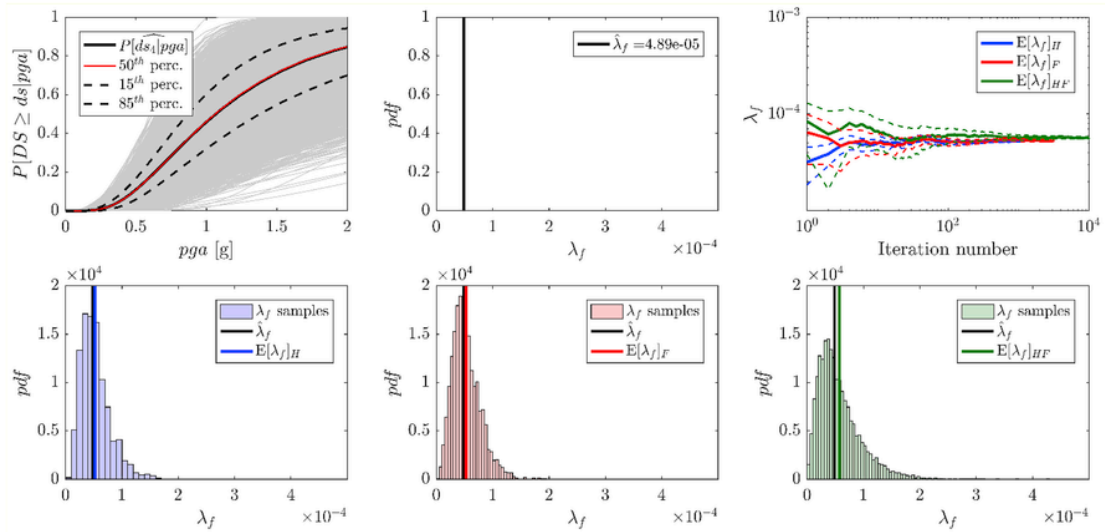
Table 4
RC arch bridge seismic reliability results.

| Parameter	Slight Damage			Moderate Damage			Extensive Damage			Complete Damage		
$\widehat{\lambda}_f$	3.27E-03			1.00E-03			2.53E-04			4.89E-05		
Uncertainty case	H	F	HF	H	F	HF	H	F	HF	H	F	HF
a_G	22.592	8.434	6.441	14.110	9.428	5.836	7.524	7.634	3.960	4.367	4.447	2.303
b_G	1.46E-04	4.22E-04	5.39E-04	7.11E-05	1.13E-04	1.83E-04	3.46E-05	3.52E-05	7.01E-05	1.20E-05	1.19E-05	2.48E-05
μ_{Λ_f}	3.31E-03	3.56E-03	3.47E-03	1.00E-03	1.06E-03	1.07E-03	2.60E-04	2.69E-04	2.78E-04	5.26E-05	5.31E-05	5.70E-05
δ_{Λ_f}	0.210	0.344	0.394	0.266	0.326	0.414	0.365	0.362	0.502	0.479	0.474	0.659
$\lambda_{f,k}$	4.53E-03	5.79E-03	5.99E-03	1.48E-03	1.69E-03	1.89E-03	4.34E-04	4.46E-04	5.40E-04	9.97E-05	1.00E-04	1.29E-04
$\lambda_{f,k}/\widehat{\lambda}_f$	1.385	1.769	1.831	1.472	1.680	1.878	1.713	1.762	2.132	2.041	2.051	2.650
$\beta_{E,\mu,1}$	2.715	2.691	2.700	3.090	3.073	3.070	3.470	3.461	3.452	3.878	3.786	3.859
$\beta_{E,\kappa,1}$	2.610	2.525	2.513	2.972	2.931	2.896	3.330	3.323	3.269	3.720	3.719	3.654
$\beta_{target,1}$	2.9 - Serviceability			2.9 - Serviceability			4.7 - Ultimate			4.7 - Ultimate		
Safety check	✗	✗	✗	✓	✓	✗	✗	✗	✗	✗	✗	✗
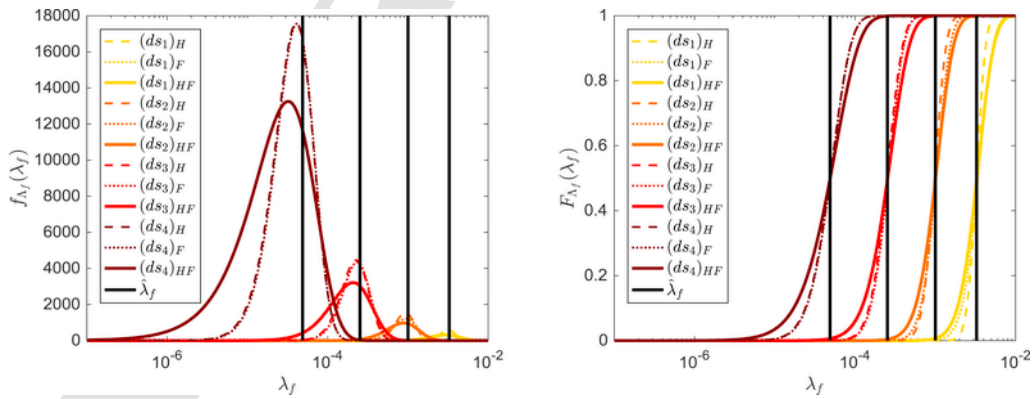
Fig. 15. Failure rate *pdfs* $f_{\Lambda_f}(\lambda_f)$ and *cdfs* $F_{\Lambda_f}(\lambda_f)$ fitted for each DS for all H, F and HF uncertainty cases.

lowing form [50]:

$$P\left[f|im\right] = P\left[EDP > \overline{edp}\middle|im\right] = 1 - P\left[EDP \le \overline{edp}\middle|im\right] = 1 - \Phi\left[\frac{ln\left(\overline{edp}\right) - ln}{\beta}\right]$$

In Eq. (10), $\overline{edp}$ is the median value of the assumed structural limit state, and edp represents the median estimate of the demand that can be computed with a ln-linear regression model as:

$$ln\left(edp\right) = a_1 + a_2 \cdot ln\left(im\right) \tag{11}$$

Finally, β is the standard deviation of the demand conditioned on im and can be estimated from the regression of the seismic demands as

$$\beta = \sqrt{\frac{\sum_{i=i}^{n}\left[ln\left(edp_i\right) - \left(a + b \cdot ln\left(im_i\right)\right)\right]^2}{n-2}} \tag{12}$$

Note that this model assumes a deterministic capacity, and consequently with a standard deviation equal to 0. When treating a_1, a_2 and β as RVs, the fragility itself becomes random and Eq. (13) can be rewritten as:

$$P\left[f|im;\boldsymbol{\Theta}_F\right] = 1 - \Phi\left[\frac{ln\left(\overline{edp}\right) - ln\left(a_1 + a_2 \cdot ln\left(im\right)\right)}{\beta}\right] \text{with } \boldsymbol{\Theta}_F = \left[A_1, A_2, B\right]$$

Parameters a, b and β are commonly estimates from n couples of points $\left[ln\left(im_i\right), ln\left(edp_i\right)\right]$ obtained from structural analysis, and thus it makes the structural fragility itself an estimate $P\left[f|im;\widehat{\boldsymbol{\Theta}}_F\right]$. Finally, since the estimates of A_1, A_2 and B are computed with a linear regression, the moments of these three estimators are known [59] and are provided by the following equations:

$$VAR\left[\widehat{a}_1\right] \approx \left(\frac{1}{n} + \frac{\widehat{m}^2}{\sum_{i=1}^{n}\left[log\left(im_i\right) - \widehat{m}\right]^2}\right) \cdot \widehat{\beta}^2 \tag{14}$$

$$VAR\left[\widehat{a}_2\right] \approx \frac{\widehat{\beta}^2}{\sum_{i=1}^{n}\left[log\left(im_i\right) - \widehat{m}\right]^2} \tag{15}$$

$$COV\left[\widehat{a}_1, \widehat{a}_2\right] \approx \frac{-\widehat{m} \cdot \widehat{\beta}^2}{\sum_{i=1}^{n}\left[log\left(im_i\right) - \widehat{m}\right]^2} \tag{16}$$

$$VAR\left[\widehat{\beta}^2\right] \approx \frac{2 \cdot \widehat{\beta}^4}{n-2} \tag{17}$$

where $\widehat{m} = \frac{1}{n}\sum_{i=1}^{n}log\left(im_i\right)$, i.e. the mean of the im_i values of the records used for the structural analysis.

3. Proposed new seismic reliability indexes

This Section formalizes the dependence of $\lambda_f(\boldsymbol{\Theta})$ on model parameters and illustrates the newly proposed seismic reliability indexes. As widely shown in the previous sections, the failure rate λ_f is function of series of uncertain parameters that are involved in both the hazard and fragility computation. As a consequence, Eq. (1) can be re-written in a more general way, as:

$$\lambda_f(\boldsymbol{\Theta}) = \int_{im} P\left[f|im;\boldsymbol{\Theta}_F\right] \cdot \left|d\lambda_{im};\boldsymbol{\Theta}_H\right| \tag{18}$$

for highlighting the randomness of the failure rate itself, and its dependence on the two uncertainty sources. At this point, $\lambda_f(\boldsymbol{\Theta})$ can be computed in three possible ways, depending on the level of required accuracy and available information. The simplest case (and the most common) is represented by a point estimate of $\widehat{\lambda}_f$, obtained for specific values of the model parameters ($\boldsymbol{\Theta} = \widehat{\boldsymbol{\Theta}}$), usually the mean or the median value of the model parameters distributions, in the following way:

$$\widehat{\lambda}_f = \lambda_f\left(\widehat{\boldsymbol{\Theta}}\right) = \int_{im} P\left[f|im;\widehat{\boldsymbol{\Theta}}_F\right] \cdot \left|d\lambda_{im};\widehat{\boldsymbol{\Theta}}_H\right| \tag{19}$$

The second level of knowledge is represented by considering the two main sources of uncertainty represents separately. In this case, the expected value of the failure rate $E[\lambda_f(\boldsymbol{\Theta})]$ can be assessed by integrating $\lambda_f(\boldsymbol{\Theta})$ over the considered parameters' distributions $f(\boldsymbol{\Theta})$, and assuming specific values for the others. When considering uncertainties arising from the parameters involved in the hazard computation $\boldsymbol{\Theta}_H$, the integral is the following:

$$E\left[\lambda_f(\boldsymbol{\Theta})\right]_H = \int \lambda_f\left(\widehat{\boldsymbol{\Theta}}_F, \boldsymbol{\Theta}_H\right) f\left(\boldsymbol{\Theta}_H\right) d\boldsymbol{\Theta}_H = \int \left\{\int_{im} P\left[f|im;\widehat{\boldsymbol{\Theta}}_F,\right] \cdot \left|d\lambda_{im};\boldsymbol{\Theta}\right.\right.$$

Similarly, the complementary formula, for uncertainty arising from the fragility parameters is:

$$E\left[\lambda_f(\boldsymbol{\Theta})\right]_F = \int \lambda_f\left(\boldsymbol{\Theta}_F, \widehat{\boldsymbol{\Theta}}_H\right) f\left(\boldsymbol{\Theta}_F\right) d\boldsymbol{\Theta}_F = \int \left\{\int_{im} P\left[f|im;\boldsymbol{\Theta}_F\right] \cdot \left|d\lambda_{im};\widehat{\boldsymbol{\Theta}}_H\right.\right.$$

The third level of knowledge allows considering all the possible sources of uncertainty, both in the hazard and fragility curve. In the most general case, the expected value of the seismic failure rate $E[\lambda_f(\boldsymbol{\Theta})]_{HF}$ is provided by the following equation:

$$E\left[\lambda_f(\boldsymbol{\Theta})\right]_{HF} = \int \lambda_f(\boldsymbol{\Theta}) f(\boldsymbol{\Theta}) d\boldsymbol{\Theta} = \int \left\{\int_{im} P\left[f|im;\boldsymbol{\Theta}_F\right] \cdot \left|d\lambda_{im};\boldsymbol{\Theta}_H\right.\right\} f(\boldsymbol{\Theta}) d$$

Since most of times $\boldsymbol{\Theta}$ is a vector composed by several parameters, and, its mathematical form of λ_{im} is not *a-priori* known, the computation of Eqs. 20–22 can be difficult in a close analytical way. For this reason, suitable simulation methods, as the Monte Carlo Simulation (MCS), are required. In this case, the result accuracy is important, and may be measured and checked, by setting a suitable threshold value for the coefficient of variation (C.O.V.) of the solution. This procedure allows obtaining an adequate number of $\lambda_{f,i}$ samples, and thus drawing the (pdf) of the failure rate $f_{\Lambda_f}(\lambda_f)$, by fitting the samples with a suitable known function.

The failure rate distribution $f_{\Lambda_f}(\lambda_f)$ represents the most complete information on the seismic reliability of a structural system, and starting from this, new seismic reliability indexes are defined in order to provide a clear and synthetic description of the seismic reliability and its accuracy. First, the *Expected Failure Rate* μ_{Λ_f} representing the weighted average of the Λ_f RV, can be derived as:

$$\mu_{\Lambda_f} = E\left[\Lambda_f\right] = \int \lambda_f \cdot f_{\Lambda_f}\left(\lambda_f\right) d\lambda_f \tag{23}$$

Then *Failure Rate Dispersion* δ_{Λ_f} can be computed as a measure of the degree of dispersion of the failure rate distribution, derived as the coefficient of variation of Λ_f. This indicator is preferred to the common variance (or standard deviation) since the measure of variability is more meaningful if measured relative to the central value, and μ_{Λ_f} is always positive:

$$\delta_{\Lambda_f} = \frac{\sigma_{\Lambda_f}}{\mu_{\Lambda_f}} = \frac{\sqrt{\int \int \left(\lambda_f - \mu_{\Lambda_f}\right)^2 \cdot f_{\Lambda_f}\left(\lambda_f\right) d\lambda_f}}{\int \lambda_f \cdot f_{\Lambda_f}\left(\lambda_f\right) d\lambda_f} \quad (24)$$

Hence, in analogy with the philosophy of semi-probabilistic structural safety approach, the *Characteristic Failure Rate* $\lambda_{f,k}$ is introduced as the failure rate value, whose probability of being exceeded is 5%, and computed as:

$$\lambda_{f,k} = F_{\Lambda_f}^{-1}(0.95) \quad (25)$$

where $F_{\Lambda_f}^{-1}(0.95)$ is the inverse of the cumulative density function CDF of the RV Λ_f.

Finally, in order to allow a direct comparison with target structural safety values provided in the current technical codes for constructions, other two new seismic reliability indexes are introduced using the actual metric for reliability analysis, namely *Center of Seismic Reliability* $\beta_{E,\mu,t}$ and *Characteristic Seismic Reliability* $\beta_{E,k,t}$ indexes, computed respectively as follows:

$$\beta_{E,\mu,t} = -\Phi^{-1}\left(1 - e^{-\mu_{\Lambda_f} t}\right) \quad (26)$$

$$\beta_{E,k,t} = -\Phi^{-1}\left(1 - e^{-\lambda_{f,k} t}\right) \quad (27)$$

where t is the target time window of interest and the subscript "E" stands for "earthquake". The final seismic safety check, that needs to be performed in order to confirm the seismic reliability of a structural system, can be expressed as:

$$\beta_{E,k,t} \geq \beta_{target} \quad (28)$$

where β_{target} represents the target structural reliability to be fulfilled during the time window of interest.

4. Application to a bridge case study

In this Section, a detailed illustration of a case study is provided, further used for applying the proposed general approach to seismic reliability assessment. The proposed general approach has been applied to an existing single-span open-spandrel RC arch bridge located in the Vicenza district (lat. 46.01, lon. 11.63), northeastern Italy. Five RC arches of 60 m span, 5.5 m arch rise and a transversal spacing of 3 m, each one with a rectangular section of 1 m height and 0.5 m width, characterize the bridge. RC arches are connected with RC arch transverse beams placed at the arches axes with a longitudinal spacing of 6 m, and a rectangular section of 0.3 m height and 0.6 m width. RC piers, with a square section of 0.3 m side and placed on each RC arch with a longitudinal spacing of 6 m, sustain the girder composed by a grillage of RC beams. In particular, longitudinal deck RC beams are characterized by a rectangular section of 0.5 m height and 0.3 m width, whereas transversal beams are realized with a rectangular section of 0.4 m height and 0.3 m width. The RC beam grillage supports a 0.2 m thickness RC slab constituting the roadway surface, and bounded with marble parapets. Fig. 1 shows main geometrical features, i.e. elevation, and longitudinal and transversal sections of the analyzed RC arch bridge.

For the classic seismic reliability assessment, a PSHA and a seismic fragility analysis have been conducted. The seismogenic source zone model ZS9 detailed in Meletti et al. [60] has been adopted, using Gutenberg-Richter (G-R) recurrence laws for each of the six SZs considered (i.e. SZs # 903, # 904, # 905, # 906, # 907 and # 912). Main G-R parameters (i.e., mean annual rate of events with magnitude above

the minimum magnitude value $\nu_{m_{min,i}}$, slope coefficient b, minimum magnitude value m_{min} and maximum magnitude value m_{max}) are listed in Table 1 (mean values), as reported in Barani et al. [61]. As regards the ground motion prediction equation (GMPE) model, the formulation proposed by Bindi et al. [62] has been adopted, considering a type-B soil class ($V_{S30} = 360$–800 m/s) on the basis of available information on the local stratigraphy. Fig. 2 maps the bridge site with respect to the six SZs considered, and the resulting seismic hazard curve, highlighting how SZs # 905 and # 906 mostly contribute to the hazard of the bridge site.

Seismic fragility analysis has been conducted performing a set of non-linear time history analyses (NLTHAs) on a 3-D finite element (FE) model of the analyzed RC arch bridge. The 3-D FE model has been implemented in Seismostruct software platform [63] in order to properly characterize main structural features of the analyzed bridge for the following seismic reliability analysis purposes. In particular, frame elements (i.e. arches, piers and arch transverse beams) have been modelled using distributed plasticity fiber-section elements with force-based formulation, whereas deck RC grillage beams (both longitudinal and transversal) have been modelled as elastic elements. Deck RC grillage beams are connected through rigid links to the RC slab, which is realized with a rigid diaphragm constraint type. Fig. 3 shows a 3-D view of the FE model of the RC arch bridge, with information on longitudinal reinforcement and stirrups in each structural element, discretization of fiber cross-sections for non-linear RC elements, and adopted constitutive laws for unconfined and confined concrete and steel reinforcement bars.

In particular, in order to take into account the confinement action, two different stress-strain laws have been assigned to the core and cover concrete fibers, respectively. A cylindrical compressive strength $f_{c0} = 25$ MPa has been considered in correspondence of a peak strain $\varepsilon_{c0} = 0.002$ and an ultimate strain value $\varepsilon_{cu} = 0.0035$ for the unconfined concrete. The confinement model of Mander et al. [64] has been instead considered for the confined concrete, with cylindrical compressive strength $f_{cc0} = 33$ MPa in correspondence of increased peak strain $\varepsilon_{cc0} = 0.0033$ and ultimate strain $\varepsilon_{cu} = 0.008$ values. As regards the constitutive law for steel rebars, the Menegotto-Pinto steel model [65] coupled with the isotropic hardening rules proposed by Filippou et al. [66] has been used, considering a yielding stress $f_{ys} = 483$ MPa and elastic modulus $E_s = 200000$ MPa, with strain hardening parameter equal to 0.005. The RC arch bridge FE model has been fixed with restraints at the arches' supports, considering the dead loads of all the structural elements as masses.

A preliminary eigenvalue analysis has been carried out in order to understand the dynamic behavior of the bridge, with the further aim to identify the engineering demand parameter to be monitored in the following reliability analysis. Fig. 4 portrays the first 10 vibration modes of the RC arch bridge, listing for each the period T_i and the effective modal mass percentage (EMMP).

Results show how the dynamic response is mainly governed by the first transversal (Y-axis) vibration mode $T_1 = 0.594$ s, with $T_4 = 0.262$ s and $T_7 = 0.189$ s being the other relevant modes in vertical direction (Z-axis), whereas no significant ones have been observed in the longitudinal direction (X-axis). Some notable rotational vibration modes have been detected also along the longitudinal (i.e. T_5 and T_8) and vertical (i.e. T_3 and T_6) axes. Based on these evidences, the 2-D interstory drift ratio (IDR) of the first external RC pier with 6 m height has been considered as relevant engineering demand parameter:

$$IDR(\tau)$$
$$= \frac{\sqrt{\left[u_{B,x}(\tau) - u_{A,x}(\tau)\right]^2 + \left[u_{B,y}(\tau) - u_{A,y}(\tau)\right]^2}}{h} \quad (29)$$

with $u_{B,i}(\tau)$ and $u_{A,i}(\tau)$ the absolute displacement of top (B) and bottom

(A) nodes of the pier along X-, Y— at a τ^{-th} generic time instant, and h the pier height.

A set of 30 natural 3-D seismic records has been collected from the European Strong Motion Database [67], and further used to execute the NLTHAs. Table 2 lists main information in terms of magnitude, epicentral distance, horizontal (i.e. the X—Y resultant) and vertical peak ground acceleration (PGA) values for each seismic record.

NLTHAs have been subsequently run, extracting 3-D interstory drift ratios time histories, and thus deriving the maximum IDR value of the first external RC pier with 6 m height for each record. Cloud analysis method has been then used to derive the seismic fragility curves of the analyzed RC arch bridge, expressed in terms of horizontal PGA. Results derived from NLTHAs have been fitted in the bi-logarithmic plane according to Eq. (11), thus deriving $\hat{a}_1$ and $\hat{a}_2$ coefficient of the ln-linear regression model and the standard deviation $\hat{\beta}^2$ via Eq. (12), and equal to -3.979, 1.055 and 0.42, respectively. Four different damage states (i.e. Slight, Moderate, Extensive and Complete Damage) has been fixed considering IDR thresholds equal to 0.25%, 0.5%, 1% and 2% respectively, thus leading to derive four fragility curves computed with Eq. (10). Fig. 5 shows the results of Cloud Analysis with NLTHA data points, the assumed IDR thresholds and resulting set of fragility curves.

5. Results

The present Section shows the results obtained from the application of the proposed general approach to the seismic reliability assessment. Once run PSHA and fragility analysis, the failure rate of the RC arch bridge has been first computed via the classic seismic failure rate estimation with Eq. (19). Considering, as illustrative example, the Complete Damage State (Fig. 6), the seismic reliability assessment leads to a point estimate of the seismic failure rate equal to $\hat{\lambda}_f = 4.89E-05$.

Hence, seismic reliability analysis has been performed with the proposed general approach accounting for uncertainties both in hazard and fragility models. Table 1 lists main data for the uncertainty characterization of hazard model parameters Θ_H, providing mean, C.O.V. values and distribution type for each input parameter, and used in the computation of hazard curve samples $\lambda_{im}(\Theta_H)$ with Eq. (4). In the same way, Table 3 lists main data for the uncertainty characterization of fragility model parameters Θ_F, providing mean, C.O.V. values and distribution type for each input parameter and correlation coefficient between a_1 and a_2 parameters. Fig. 7 shows Θ_F samples subsequently used to derive fragility curve realizations $P[f|im;\Theta_F]$ with Eq. (13).

MCS technique has been then used to compute an adequate number of failure rate samples $\lambda_{f,i}$, setting an adequate and high accuracy level, ensured by the fulfilment of a C.O.V. of the solution smaller than to 2%. Fig. 8 shows failure rate samples obtained considering H, F, and HF uncertainties, highlighting how a higher dispersion characterizes the F case with respect to the H one, and increases in the combined HF case. Fig. 9 illustrates the number of iterations required to fulfill MCS convergence criterion, highlighting how the number of samples needed in the HF case is between 4 and 10 times higher than the one required for F and H ones.

The failure rate samples $\lambda_{f,i}$ have been subsequently used to fit failure rate pdf $f_{\Lambda_f}(\lambda_f)$: in this specific case, a Gamma distribution has been choosen as suitable function, as follows:

$$f_{\Lambda_f}(\lambda_f) = \frac{1}{b_G{}^{a_G}\Gamma(a)} \lambda_f{}^{a_G-1} e^{-\frac{\lambda_f}{b_G}} \tag{34}$$

where $\Gamma(\cdot)$ is the Gamma function, a_G is the shape parameter and b_G the scale parameter. Main Gamma distribution parameters a_G, b_G have been derived, and are equal to 4.367 and 1.20E-05 for the H case, 4.447 and 1.19E-05 for the F case, and 2.303 and 2.48E-05 for the HF case. Fig. 10 represents the fitted failure rate pdfs, highlighting the

good fitting of the selected functional form with the comparison between the cumulative density functions $F_{\Lambda_f}(\lambda_f)$ and the empirical CDF (ECDF) of the sampled data.

Once the failure rate pdf $f_{\Lambda_f}(\lambda_f)$ has been fitted, the last step consists in the computation of the new seismic reliability indexes, according to Eqs. 24–27. First, the *Expected Failure Rate* μ_{Λ_f} has been derived for the abovementioned three cases, i.e. with uncertainties in only hazard (H), in only fragility (F), and in both hazard and fragility (HF), with values equal to 5.26E-05 (H), 5.31E-05 (F), and 5.70E-05 (HF), slightly higher than the benchmark case represented by the point estimate $\hat{\lambda}_f = 4.89E-05$. *Failure Rate Dispersion* δ_{Λ_f} has been then computed, resulting in estimates equal to 0.479 (H), 0.474 (F) and 0.659 (HF), thus confirming the higher level of dispersion of failure rate in the last HF case. Hence, the *Characteristic Failure Rate* $\lambda_{f,k}$ (i.e. the failure rate value whose probability of being exceeded is 5%) has been calculated, leading to estimates equal to 9.97E-05 (H), 1.00E-04 (F), and 1.29E-04 (HF). It is worth noting how the ratio $\lambda_{f,k}/\hat{\lambda}_f$ between the *Characteristic Failure Rate* $\lambda_{f,k}$ and the point estimate of the seismic failure rate derived with the classic approach $\hat{\lambda}_f$ is equal to 2.041, 2.051 and 2.65 in the H, F and HF cases, respectively, thus evidencing how in the specific case $\lambda_{f,k}$ has values larger than twice of the $\hat{\lambda}_f$ point estimate derived with the current classic seismic reliability assessment approach.

On those bases, the final seismic reliability indexes *Center of Seismic Reliability* $\beta_{E,\mu,t}$ and *Characteristic Seismic Reliability* $\beta_{E,k,t}$ have been derived according to Eqs. (30–31), considering a 1-year target time window, and resulting in $\beta_{E,\mu,1}$ values equal to 3.878 (H), 3.786 (F), 3.859 (HF) and $\beta_{E,k,1}$ estimates of 3.72 (H), 3.719 (F), 3.654 (HF), respectively. Lastly, considering a yearly target structural reliability $\beta_{target,1}$ equal to 4.7 [68] for the Ultimate Limit State, the structural safety assessment carried out with Eq. (32) is not fulfilled, thus requiring further efforts in designing a seismic retrofit project for the analyzed RC arch bridge structure.

6. Discussion

In this Section, an in-depth discussion of the results obtained from the case study aimed at highlighting the prevailing source of randomness, and the impact of such uncertainties when looking to different damage states is carried out. A further set of seismic reliability analyses has been performed with the proposed general approach, in order to investigate the role of hazard and fragility uncertainties on the failure rate pdf $f_{\Lambda_f}(\lambda_f)$ related to different Damage States. Figs. 11–14 illustrates the results for H, F, and HF uncertainty cases with reference to Slight, Moderate, Extensive and Complete Damage State respectively. Figs. 11–14 present for each DS the sampled fragility curves, the seismic failure rate derived with the classic approach $\hat{\lambda}_f$, the number of iterations required to reach MCS convergence, and failure rate samples $\lambda_{f,i}$ further used to fit H, F and HF failure rate pdfs $f_{\Lambda_f}(\lambda_f)$. Gamma distributions have been used as functional form for all the investigated DS, with fitted a_G and b_G parameters listed in Table 4. Fig. 15 shows failure rate pdfs $f_{\Lambda_f}(\lambda_f)$ and cdfs $F_{\Lambda_f}(\lambda_f)$ fitted for each DS for all H, F and HF uncertainty cases, and compared with respective $\hat{\lambda}_f$ point estimates. Results show how dispersion related to uncertainty is the highest for the HF case for each DS, i.e. when both hazard and fragility sources on uncertainty are accounted, whereas in the specific analyzed case study, uncertainty coming from fragility (F) is higher than that associated to hazard model parameters (H). Hence, μ_{Λ_f}, δ_{Λ_f}, $\lambda_{f,k}$ and the ratio $\lambda_{f,k}/\hat{\lambda}_f$, have been computed for each DS, and listed in Table 4. Results of the seismic reliability assessment show how for increasing DS a decrease of the *Expected Failure Rate* μ_{Λ_f} is observed, but at the same time an increase of the *Failure Rate Dispersion* δ_{Λ_f}, with values from 0.394 (HF - Slight DS) to 0.659 (HF – Complete DS), even if, in absolute terms, the range of failure rate samples $\lambda_{f,i}$, is higher for less severe DSs. A general

trend can be captured also for the ratio $\lambda_{f,k}/\hat{\lambda}_f$, with growing values from H to F and HF uncertainty cases in each DS, and increasing values among different DSs, from Slight DS (ranging between 1.385 and 1.831) to Complete DS (with values between 2.041 and 2.650).

The final seismic reliability indexes *Center of Seismic Reliability* $\beta_{E,\mu,1}$ and *Characteristic Seismic Reliability* $\beta_{E,k,1}$ for a yearly target time window have been computed for each DS, showing decreasing values for additional uncertainties in each DS, and an increasing trend from Slight DS to Complete DS. Lastly, a structural safety check have been conducted for each investigated uncertainty case and DS, comparing yearly *Characteristic Seismic Reliability* $\beta_{E,k,1}$ values with related $\beta_{target,1}$ reference estimates. Two different $\beta_{target,1}$ values have been considered, related to Serviceability Limit State ($\beta_{target,SLS,1} = 2.9$) and Ultimate Limit State ($\beta_{target,ULS,1} = 4.7$) [68], considering Slight and Moderate DSs linked to Serviceability Limit State, whereas both Extensive and Complete DSs related to Ultimate Limit State. Table 4 lists structural safety checks outcomes, highlighting how, for Serviceability Limit State H and F Moderate DS fulfills structural safety, whereas the analyzed RC arch bridge is not safe with respect to Ultimate Limit State in both Extensive and Complete DSs, thus suggesting further efforts in designing an effective seismic retrofit project.

7. Conclusions

The present work illustrated a novel general approach for the assessment of seismic reliability of structural systems able to account for underlying uncertainties in the definition of the input parameters of seismic hazard and fragility models. This study showed how the use of the classic approach for computing seismic reliability leads to a point estimate of the failure probability for a DS of interest, without knowledge of the level of uncertainty characterizing it. A set of new seismic reliability indexes was therefore defined, namely *Expected Failure Rate, Failure Rate Dispersion, Characteristic Failure Rate, Center of Seismic Reliability* and *Characteristic Seismic Reliability*. In particular, the *Characteristic Failure Rate* $\lambda_{f,k}$ represents an assumed safety margin that can be used by engineers and risk practitioners for managing uncertainty arising from both hazard and fragility sides. The only point estimate $\hat{\lambda}_f$ provides is fact only a partial (and therefore limited) knowledge of the structural safety, since it can be strongly influenced by multiple uncertainty sources. The adoption of such formal indicator allows engineers to consider the failure rate itself as a random variable due to epistemic uncertainties and thus extracting statistically significant values corresponding to a specific quantile, in analogy to how materials' and loads' properties are taken into account in current structural safety codes [12–14]. In addition, together with the *Failure Rate Dispersion* δ_{Λ_f}, $\lambda_{f,k}$ may thus represent an important information for decision makers dealing with the assessment of seismic reliability considering potential variability of λ_f due to models and parameters uncertainties. Similar considerations are of course valid also for the *Characteristic Seismic Reliability* $\beta_{E,k,t}$, due to its direct dependence from $\lambda_{f,k}$.

In other terms, the proposed general approach allows quantifying the degree of belief that the risk analyst has for a certain seismic reliability estimate, and this is a key step for a future rational seismic reliability analysis practice. The main aim of earthquake engineering researchers nowadays should be in fact to formalize clear and reproducible risk and reliability analysis procedures, with the aim to characterize as much as possible the "real" seismic reliability of a structural system and to be able to easily communicate analysis results also to non-technical audience.

The proposed general approach was then used in a practical application of seismic reliability assessment, considering as case-study an existing open-spandrel RC arch bridge. The analyses were carried out considering 4 different mutually-exclusive collectively exhaustive damage states (i.e. Slight, Moderate, Extensive and Complete DS), and ana-

lyzing the impact of uncertainties in hazard and fragility, considering 3 different uncertainty cases (H, F and HF). Even if results are case-study sensitive, some general remarks can be done:

- Uncertainty in fragility curve fitting is relevant and comparable to that associated all input parameters required in computing hazard curves;
- The highest dispersion in failure rate samples is observed considering the HF case;
- Failure rate *pdfs* $f_{\Lambda_f}(\lambda_f)$ are characterized by higher *Failure Rate Dispersion* δ_{Λ_f} values for the most severe DSs, thus requiring a higher number of samples for the MCS convergence criterion fulfilment;
- The present application considered only epistemic inter-model uncertainty, due to uncertainty in model parameters, but the proposed general approach allows also to take into account inter-models uncertainty for describing the uncertainty among different models, with the use of further MCS cycles.

Appendix A. Supplementary data

Supplementary data to this article can be found online at https://doi.org/10.1016/j.soildyn.2019.04.028.

References

[1] P. Castaldo, M. Calvello, B. Palazzo, Probabilistic analysis of excavation-induced damages to existing structures, Comput Geotech 53 (2013) 17–30.

[2] G.I. Schueller, R. Stix, A critical appraisal of methods to determine failure probabilities, Struct Saf 4 (1987) 293–309.

[3] J.C. Mitteau, Error evaluations for the computation of failure probability in static structural reliability problems, Probabilist Eng Mech 14 (1999) 119–135.

[4] P. Castaldo, F. Jalayer, B. Palazzo, Probabilistic assessment of groundwater leakage in diaphragm wall joints for deep excavations, Tunn Undergr Space Technol 71 (2018) 531–543.

[5] A. Harbitz, An efficient sampling method for probability of failure calculation, Struct Saf 3 (1986) 109–115.

[6] G.I. Schueller, C.G. Bucher, U. Bourgund, W. Ouypornprasert, On efficient computational schemes to calculate failure probabilities, Probabilist Eng Mech 4 (1989) 10–18.

[7] O. Ditlevsen, H.O. Madsen, Structural reliability methods, John Wiley and Sons, Chichester, 1996.

[8] S.K. Au, J.L. Beck, Estimation of small failure probabilites in high dimensions by subset simulation, Probabilist Eng Mech 16 (2001) 263–277.

[9] A. Florian, An efficient sampling scheme: updated Latin Hypercube Sampling, Probabilist Eng Mech 7 (1992) 123–130.

[10] D.E. Huntington, C.S. Lyrintzis, Improvements to and limitations of Latin hypercube sampling, Probabilist Eng Mech 13 (1998) 245–253.

[11] P. Castaldo, G. Mancini, B. Palazzo, Seismic reliability-based robustness assessment of three-dimensional reinforced concrete systems equipped with single-concave sliding devices, Eng Struct 163 (2018) 373–387.

[12] European Committee for Standardization (CEN), EN 1990, eurocode 0 – basis of structural design, 2004, [Brussels].

[13] Joint Committee on Structural Safety (JCSS), Probabilistic model code, 12th draft JCSS – joint committee on structural safety, 2001.

[14] International Organization for Standardization (ISO), ISO 2394, general principles on reliability for structures, 2015, [Switzerland].

[15] J.J. Bommer, Uncertainty about the uncertainty in seismic hazard analysis, Eng Geol 70 (1–2) (2003) 165–168.

[16] A. Rebez, D. Slejko, Introducing epistemic uncertainties into seismic hazard assessment for the broader Vittorio Veneto area, Boll Geofis Teor Appl 45 (4) (2004) 305–320.

[17] J.M. Gaspar-Escribano, A. Rivas-Medina, H. Parra, L. Cabanas, B. Benito, S. Ruiz Barajas, J.M. Martinez Solares, Uncertainty assessment for the seismic hazard map of Spain, Eng Geol 199 (2015) 62–73.

[18] R.B. Kulkarni, R.R. Youngs, K.J. Coppersmith, Assessment of confidence intervals for results of seismic hazard analysis, In: Proceedings of the eighth world conference on earthquake engineering, vol. 1, 1984, pp. 263–270, San Francisco.

[19] E.H. Field, R.J. Arrowsmith, G.P. Biasi, P. Bird, T.E. Dawson, K.R. Felzer, D.D. Jackson, K.M. Johnson, T.H. Jordan, C. Madden, A.J. Michael, K.R. Milner, M.T. Page, T. Parsons, P.M. Powers, B.E. Shaw, W.R. Thatcher, R.J. Weldon II, Y. Zeng, Uniform California earthquake rupture forecast, version 3 (UCERF3)-The time-independent model, Bull Seismol Soc Am 104 (3) (2014) 1122–1180.

[20] J.J. Bommer, F. Scherbaum, The use and misuse of logic-trees in probabilistic seismic hazard analysis, Earthq Spectra 24 (2008) 997–1009.

[21] R.K. McGuire, C.A. Cornell, G.R. Toro, The case for using mean seismic hazard, Earthq Spectra 21 (2005) 879–886.

[22] R. Musson, Against fractiles, Earthq Spectra 21 (2005) 887–891.

[23] R. Musson, On the nature of logic trees in probabilistic seismic hazard assessment, Earthq Spectra 28 (2012) 1291–1296.

[24] N.A. Abrahamson, J.J. Bommer, Probability and uncertainty in seismic hazard analysis, Earthq Spectra 21 (2005) 603–607.

[25] M. Stucchi, C. Meletti, V. Montaldo, H. Crowley, G.M. Calvi, E. Boschi, Seismic hazard assessment (2003–2009) for the Italian building code, Bull Seismol Soc Am 101 (2011) 1885–1911.

[26] W. Marzocchi, M. Taroni, J. Selva, Accounting for epistemic uncertainty in PSHA, logic tree and ensamble modeling, Bull Seismol Soc Am 105 (2015) 4.

[27] W. Marzocchi, T.H. Jordan, A unified probabilistic framework for seismic hazard analysis, Bull Seismol Soc Am 107 (6) (2017) 2738–2744.

[28] J.J. Bommer, Challenges of building logic trees for probabilistic seismic hazard analysis, Earthq Spectra 28 (4) (2012) 1723–1735.

[29] F. Sabetta, A. Lucantoni, H. Bungum, J.J. Bommer, Sensitivity of PSHA results to ground motion prediction relations and logic-tree weights, Soil Dynam Earthq Eng 25 (2005) 317–329.

[30] J. Bommer, N.A. Abrahamson, Why do modern probabilistic seismic-hazard analyses often lead to increased hazard estimates?, Bull Seismol Soc Am 96 (2006) 1967–1977.

[31] T. Most, Assessment of structural simulation models by estimating uncertainties due to model selection and model simplification, Comput Struct 89 (17–18) (2011) 1664–1672.

[32] T. Haukaas, P. Gardoni, Model uncertainty in finite-element analysis: bayesian finite elements, J Eng Mech 137 (8) (2011) 519–526.

[33] P. Castaldo, D. Gino, G. Bertagnoli, G. Mancini, Partial safety factor for resistance model uncertainties in 2D non-linear finite element analysis of reinforced concrete structures, Eng Struct 176 (2018) 746–762.

[34] I.P. Christovasilis, G.P. Cimellaro, S. Barani, S. Foti, On the selection and scaling of ground motions for fragility analysis of structures, In: Proceedings of the second European conference on earthquake engineering and seismology, August 25–29, 2014, Istanbul Turkey, 2014, p. 11.

[35] L. Sousa, M. Marques, V. Silva, H. Varum, Hazard disaggregation and record selection for fragility analysis and earthquake loss estimation, Earthq Spectra 33 (2) (2017) 529–549.

[36] M.A. Zanini, L. Hofer, F. Faleschini, C. Pellegrino, The influence of record selection in assessing uncertainty of failure rates, Ingegneria Sismica 34 (4) (2017) 30–40.

[37] J.E. Padgett, R. DesRoches, Sensitivity of seismic response and fragility to parameter uncertainty, J Struct Eng 133 (12) (2007) 1710–1718.

[38] M.N. Choine, A. O'Connor, J.E. Padgett, Comparison between the seismic performance of integral and jointed concrete bridges, J Earthq Eng 19 (1) (2014) 172–191.

[39] D.H. Tavares, J.E. Padgett, P. Paultre, Fragility curves of typical as-built highway bridges in eastern Canada, Eng Struct 40 (2012) 107–118.

[40] A.B. Liel, C.B. Haselton, G.G. Deierlein, J.W. Baker, Incorporating modeling uncertainties in the assessment of seismic collapse risk of buildings, Struct Saf 31 (2009) 197–211.

[41] O.S. Kwon, A. Elnahsai, The effect of material and ground motion uncertainty on the seismic vulnerability curves of RC structure, Eng Struct 28 (2006) 289–303.

[42] M. Dolsek, Incremental dynamic analysis with consideration of modelling uncertainties, Earthq Eng Struct Dyn 38 (6) (2008) 805–825.

[43] O.C. Celik, B.R. Ellingwood, Seismic fragilities for non-ductile reinforced concrete frames – role of aleatoric and epistemic uncertainties, Struct Saf 32 (2010) 1–12.

[44] F. Scozzese, A. Dall'Asta, E. Tubaldi, Seismic risk sensitivity of structures equipped with anti-seismic devices with uncertain properties, Struct Saf 77 (2019) 30–47.

[45] L. Jiang, J. Ye, Seismic risk assessment of a 2-storey steel-sheathed CFS building considering different sources of uncertainty, Structure (Lond) 16 (2018) 347–357.

[46] C.A. Cornell, H. Krawinkler, Progress and challenges in seismic performance assessment, PEER Cent News 3 (2) (2000) 1–3.

[47] C. Cornell, Engineering seismic risk analysis, Bull Seismol Soc Am 58 (5) (1968) 1583–1606.

[48] R.K. McGuire, Probabilistic seismic hazard analysis and design earthquakes: closing the loop, Bull Seismol Soc Am 85 (5) (1995) 1275-1284.

[49] D. Vamvatsikos, C.A. Cornell, Applied incremental dynamic analysis, Earthq Spectra 20 (2) (2004) 523–553.

[50] F. Jalayer, C.A. Cornell, Direct probabilistic seismic analysis: implementing non-linear dynamic assessments, Stanford University, 2003.

[51] J.W. Baker, Efficient analytical fragility function fitting using dynamic structural analysis, Earthq Spectra 31 (1) (2015) 579–599.

[52] B. Gutenberg, C.F. Richter, Frequency of earthquakes in California, Bull Seismol Soc Am 34 (4) (1944) 185–188.

[53] J.W. Baker, An introduction to probabilistic seismic hazard analysis (PSHA), white paper, 200872, Version 1.3.

[54] P. Bazzurro, C.A. Cornell, N. Shome, J.E. Carballo, Three proposals for characterizing MDOF nonlinear seismic response, J Struct Eng 124 (11) (1998) 1281–1289.

[55] P. Castaldo, B. Palazzo, G. Alfano, M.F. Palumbo, Seismic reliability-based ductility demand for hardening and softening structures isolated by friction pendulum bearings, Struct Contr Health Monit 25 (11) (2018), e2256.

[56] L.F. Ibarra, H. Krawinkler, Global collapse of frame structures under seismic excitations, John A. Blume Earthquake Engineering Center, Stanford, CA, 2005324.

[57] K. Porter, R. Kennedy, R. Bachman, Creating fragility functions for performance-based earthquake engineering, Earthq Spectra 23 (2) (2007) 471–489.

[58] M. Ghafory-Ashtiany, M. Mousavi, A. Azarbakht, Strong ground motion record selection for the reliable prediction of the mean seismic collapse capacity of a structure group, Earthq Eng Struct Dyn 40 (6) (2010) 691–708.

[59] A.M. Mood, F.A. Graybill, D.C. Boes, Introduction to the theory of statistics, McGraw-Hill, New York, US, 1974.

[60] C. Meletti, F. Galadini, G. Valensise, A seismic source zone model for the seismic hazard assessment of the Italian territory, Tectonophysics 450 (2008) 85–108.

[61] S. Barani, D. Spallarossa, P. Bazzurro, Disaggregation of probabilistic ground motion hazard in Italy, Bull Seismol Soc Am 99 (2009) 2638–2661.

[62] D. Bindi, F. Pacor, L. Luzi, R. Puglia, M. Massa, G. Ameri, R. Paolucci, Ground motion prediction equations derived from the Italian strong motion database, Bull Earthq Eng 9 (2011) 1899–1920.

[63] SeismoSoft, SeismoStruct – a computer program for static and dynamic nonlinear analysis of frames structures, Available at: http://www.seismosoft.com, 2013.

[64] J.B. Mander, M.J.N. Priestley, R. Park, Theoretical stress-strain model for confined concrete, J Struct Eng 114 (8) (1988) 1804–1826.

[65] M. Menegotto, P.E. Pinto, Method of analysis for cyclically loaded reinforced concrete plane frames including changes in geometry and non-elastic behavior of elements under combined normal force and bending, Proceedings IABSE symposium of resistance and ultimate deformability of structures acted on by well defined repeated loads, vol. 13, International Association of Bridge and Structural Engineering, Lisbon, Portugal, 197315–22.

[66] F.C. Filippou, E.P. Popov, V.V. Bertero, Effects of bond deterioration on hysteretic behaviour of reinforced concrete joints. Report EERC 83-19, Earthquake Engineering Research Center, University of California, Berkeley, 1983.

[67] L. Luzi, R. Puglia, E. Russo, W.G.5 ORFEUS, Engineering Strong Motion Database, version 1.0. Istituto Nazionale di Geofisica e Vulcanologia, Observatories & Research Facilities for European Seismology, 2016https://doi.org/10.13127/ESM, Available at: https://http://esm.mi.ingv.it/.

[68] European Committee for Standardization, Eurocode 0: basis of structural design, Structural Eurocodes, 200290, Technical Committee CEN/TC 250.